EFFECT OF THE HEAT TREATMENT ON THE MECHANICAL PROPERTIES OF A PRECIPITATION HARDENING STEEL FOR LARGE PLASTIC MOLDS

D. Firrao, P. Matteis, G. M. M. Mortarino, P. Russo Spena, M. G. Ienco, G. Pellati, M. R. Pinasco, R. Gerosa, G. Silva, B. Rivolta, M. E. Tata, R. Montanari

Continuously growing activity in the area of the engineering plastics led to the necessity of developing new low-cost, high-performance plastic mold steels. In fact, when it is necessary to fabricate large plastic components, such as bumpers and dashboards for motor vehicles, the traditionally adopted ISO 1.2738 plastic mold steel exhibits low fracture toughness and highly inhomogeneous microstructures (continuously varying from surface to core), as obtained from the pre-hardening (quenching and tempering) of large blooms. New alloys and alternative manufacturing routes may allow to obtain plastic injection molds with good mechanical, wear and weldability properties. Precipitation hardening tool steels are being proposed for such an application, yielding improved mechanical properties and lower overall costs and lead-time. A precipitation hardenable steel, developed for injection molding of large engineering polymer components, was investigated.
The microstructures and the mechanical properties of the precipitation hardenable steel bloom were investigated after the steelwork heat treatment. Moreover, the strengthening mechanism by means of aging heat treatments was examined on samples subjected either to the steelwork heat treatment only, or also to a successive laboratory heat treatment. To the purpose, X-rays diffraction and EDS analyses were carried out in order to indentify second phases electrochemically extracted from aged and not aged samples.

KEYWORDS: plastic mold steel, precipitation hardening, metallography, mechanical properties, fracture toughness, fractography

INTRODUCTION

Large steel molds are employed in injection molding processes to fabricate massive plastic automotive components (such as bumpers and dashboards), by using glass-reinforced thermoplastic polymers. During the service, several stresses act on a plastic mold: polymer's injection pressure, mechanical and thermal fatigue (a few millions of pieces can be fabricated with one mold), and wear from reinforced resin flows; stresses can be further enhanced by notch effects and by abnormal shop operations.
The molds are commonly machined from large quenched and tempered blooms, typically with 1x1 m cross-section and more than 1 m length. The ISO 1.2738 (or 40CrMnNiMo8-6-4 [1]) alloy steel grade is the most used steel. Due to the large section, blooms of the above steel exhibit after, heat treatment, inhomogeneous microstructures and mechanical properties continuously varying from the surface to the core of the bloom; impact notch strength and fracture toughness are everywhere quite low (at the 10 J and 40 MPa√m level, respectively [2]). Moreover, the ISO 1.2738 steel is difficult to weld (1.16 carbon equivalent index [3]), although weld bed deposition operations are usually necessary to modify the mold face, also to extend the service life during model revamping.
Several precipitation hardening steels have been proposed as an alternative, with the aim of yielding more uniform microstructures and better properties throughout the mold sections, and to improve weldability (a carbon content lower than 0.4% may be adopted).
The P21 [4,5] standard grade steel, for example, contains 0.2% C, 4% Ni, 1.2% Co, and lower amounts of V, Al, Mn, Si, Cr [4]; yet, most grades are proprietary and not disclosed in detail [6]. The solubilization temperature can be subcritical, as for the P21 grade [4,7] (albeit after an hypercritical annealing [7]), or hypercritical, for some proprietary grades, whereas the aging temperature is always subcritical (e.g. 530 °C for the P21 grade [4,7]), and therefore yields only very limited dimensional variations. The final (serv-

Donato Firrao, Paolo Matteis, Giovanni M. M. Mortarino, Pasquale Russo Spena
Politecnico di Torino, Italy
Maria G. Ienco, Gabriella Pellati, Maria R. Pinasco
Università di Genova, Italy
Riccardo Gerosa, Giuseppe Silva, Barbara Rivolta
Politecnico di Milano, Italy
Maria E. Tata, Roberto Montanari
Università di Roma Tor Vergata, Italy

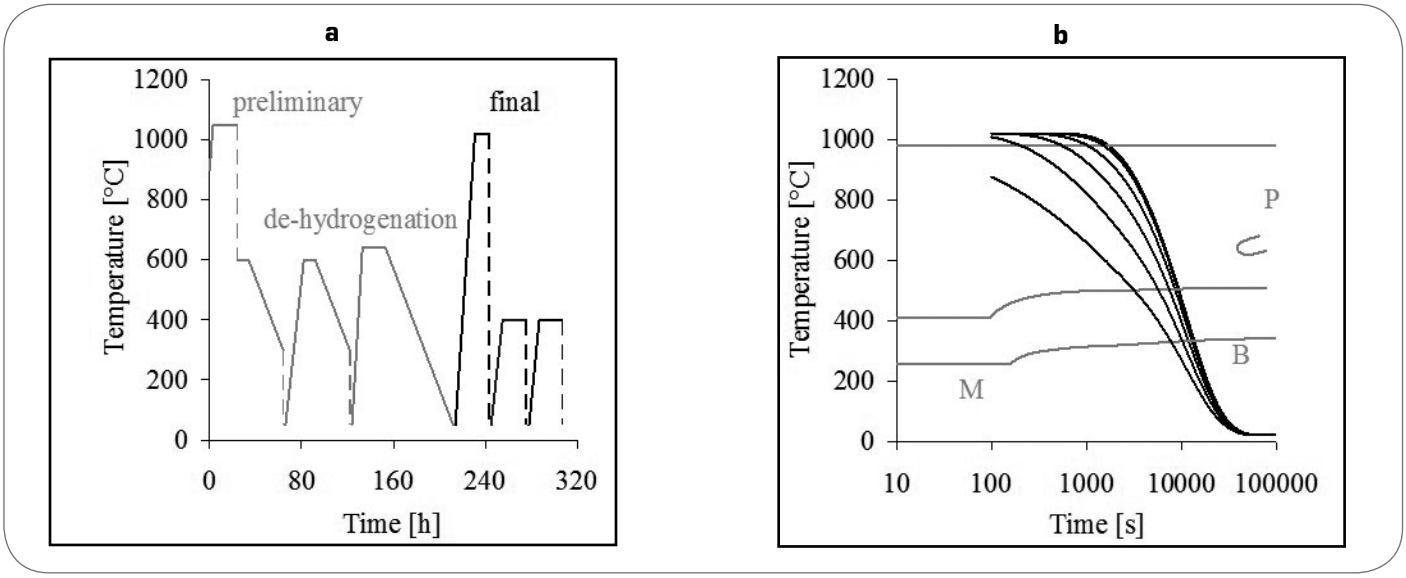

Fig. 1

Heat treatment schedule (dashed lines represent uncontrolled air cooling stages). a): Preliminary heat treatment (grey lines, including de-hydrogenation), final heat treatment (black lines). b): Bloom cooling curves from surface to core (constant-parameters analytical calculation) superimposed to the CCT diagram.

Trattamento termico complessivo (le linee tratteggiate rappresentano raffreddamenti liberi in aria). a): Trattamento termico preliminare (linee grigie, includente la de-idrogenazione), trattamento termico finale (linee nere). b): Curve di raffreddamento del blumo da superficie a cuore (calcolo analitico a parametri costanti) sovrapposte al diagramma CCT.

ice) hardness is usually in the 37-42 HRC [6] range.
The precipitation hardening heat treatment can be performed after mould machining, owing to the fact that it induces only very limited deformations [8], and a suitable aging treatment may yield homogeneous microstructures and mechanical properties in geometrically complex and large moulds. Furthermore, in some cases (e.g. for the here proposed steel), the preliminary heat-treatment performed on the as-forged bloom can employ air cooling after austenitization, as opposed to oil quenching in the case of traditional hardened steels, thus yielding much lower temperature gradients and minimizing residual stresses.
In the present work a precipitation hardenable steel is investigated; its chemical composition is listed in Tab. 1. The aging of this steel in the 550 to 630 °C temperature range was previously studied by means of hardness tests performed after increasing aging durations [9], evidencing overaging peaks after 1 or 2 h aging at 630 or 590 °C, respectively, as opposed to almost asymptotic aging at 550 °C up to 20 h duration. For this reason, and since the homogeneous heating of large moulds may require several hours and implies different actual durations at temperature from surface to core, only aging temperatures equal or lower than 550 °C are considered here.

EXPERIMENTAL PROCEDURES

The bloom production cycle, performed in the steelwork, consisted of several steps: ingot casting, hot forging (in order to reduce the microstructural and chemical inhomogeneities and to obtain a 2400 (L) x 1500 (T) x 500 (S) mm bloom), preliminary heat treatment (including a dehydrogenization process), austenitization/solubilization, air quenching, low-temperature tempering. The heat treatment schedule is displayed in Fig.1a.
By superimposing the austenite cooling stages (of the bloom heat treatment) to the steel's CCT diagram (Fig. 1b), it can be hypothesized that: i) during the first austenitization, most of the primary Mo and V carbides were dissolved; ii) during the first air cooling and furnace cooling stages, the austenite-to-pearlite transformation was avoided, a fine and homogeneous carbides re-precipitation occurred, and the austenite was finally transformed into bainite at lower temperatures, no transformation taking place in the final uncontrolled air cooling to room temperature; iii) the de-hydrogenization treatment, performed in two steps, caused (tempering and) aging of the bainitic matrix and carbides coarsening. Moreover, as it regards the final heat treatment, the bloom was austenitized at a lower temperature (1020 °C), so that Mo and V carbides were partially dissolved, and it is hypothesized that, after the air quenching, a homogeneous and fully bainitic microstructure was obtained both in the surface and in the core of the bloom. Finally, the steel was subjected to a double tempering at 400 °C.
All the examined samples were cut from the bloom at a distance of less than 170 mm from the bloom surface in the S direction.

C	Mn	Cr	Ni	Mo	Si	V
0.05 - 0.15	0.1 - 1.1	0.1 - 0.9	2.5 - 4.5	2.5 - 4.5	0.1 - 1.1	0.05 – 0.20

Tab. 1

Nominal chemical composition of the proposed steel (wt. %) (actual analysis covered by industrial confidentiality).

Composizione chimica nominale dell'acciaio proposto (% in peso) (analisi esatta coperta da riservatezza industriale).

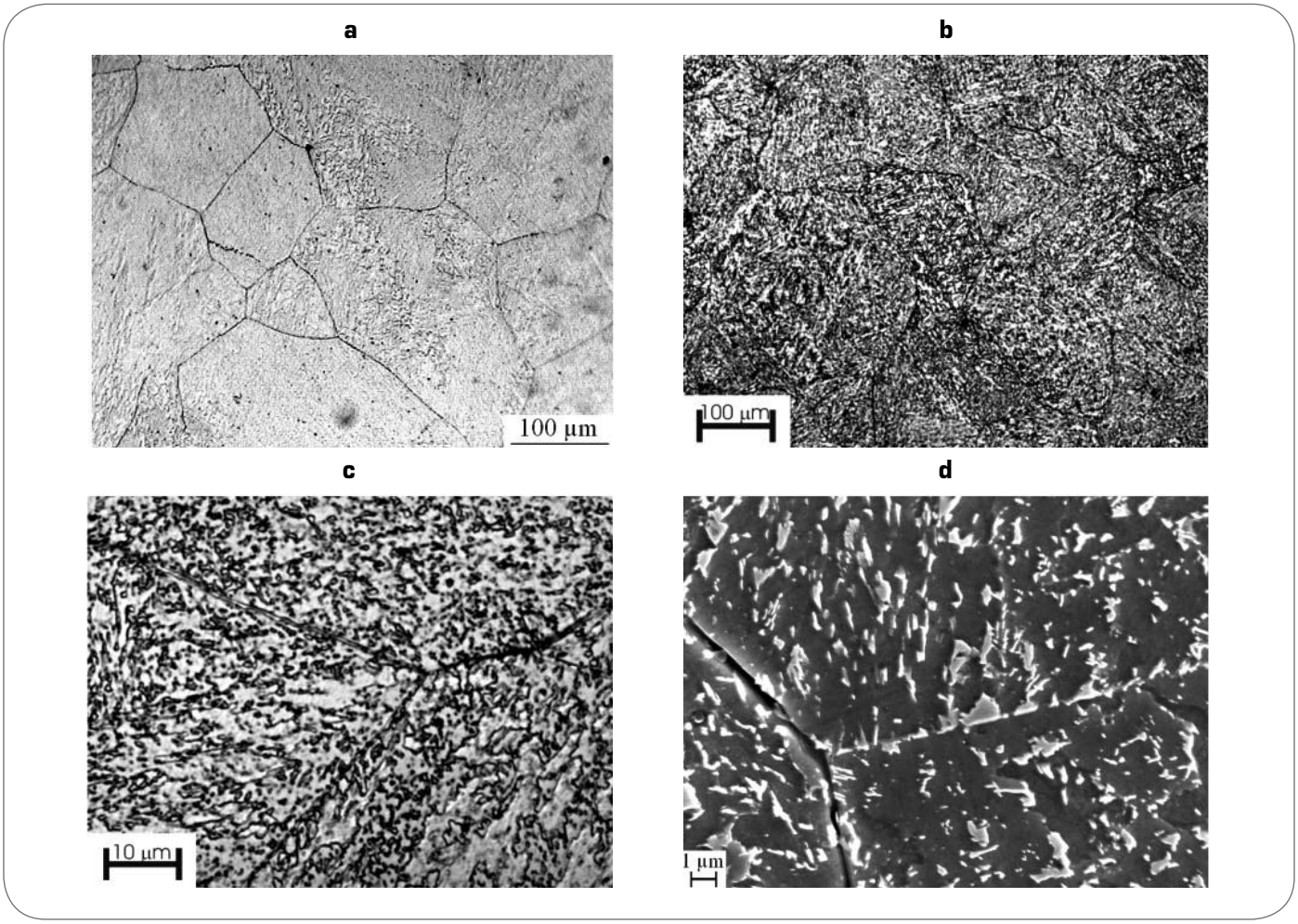

Fig. 2 ***As-received bloom microstructure: homogeneous bainite modified by tempering microscopy. Picral (a) and Nital (b,c,d) etch. Optical microscopy at increasing magnifications (a,b,c) and electron microscopy (d).***
Microstruttura del blumo allo stato di fornitura: bainite omogenea modificata dal rinvenimento. Attacco Picral (a) e Nital (b,c,d). Microscopia ottica ad ingrandimento crescente (a,b,c) e microscopi elettronica (d).

Moreover, some samples were subjected to the following laboratory re-heat-treatment: austenitization/solubilization at 1050 °C, water quenching, double tempering at 400 °C.
Sets of either as-received or laboratory re-heat-treated samples were then aged at three different temperatures: 470, 510, or 550 °C. Different samples of each set were extracted from the furnace after aging durations increasing up to 8 hours, and water quenched.
The microstructure was examined by optical and electronic microscopy, after Nital or Picral [10] etch, and the austenitic average grain size was measured by using the circular intercept method [11], after Bechet-Beaujard [12] etch.
Standard tensile tests, plain-strain fracture toughness tests, Charpy-V impact tests, Vickers hardness tests, and FIMEC (Flat top cylindrical Indentations for Mechanical Characterization) test were performed upon samples cut from the steel bloom, either in the as-received state or after the above described re-heat treatments. The reported hardness values are averages of 3 indentations. Fracture toughness tests were performed on 35 mm thick SENB (Single Edge Notch Bend) specimens [13]. The FIMEC indentation tests [14,15,16,17] were performed with a flat cylindrical indenter (1 mm diameter) and a 1.66 μm/s displacement rate. The fracture surfaces of tensile and fracture toughness samples were examined by Scanning Electron Microscopy (SEM).
X-ray diffraction and EDS analyses were performed on electrochemically extracted second phases (carbides and inclusions), in order to detect the nature of the particles precipitated during the aging heat treatment. The sample was dissolved in ethanol and hydrochloric acid (10% vol.), the undissolved second phases were collected on a filter (0.1 mm mesh size), and the filter was subjected to X-ray diffraction analysis (Co-K_α radiation). For comparison, the same analysis was carried out on an unused filter. EDS analyses was performed on compacted second phase powder.

RESULTS

Microstructures

After the steelwork heat treatment, the as-received microstructure is homogeneous bainite, modified by tempering (Fig. 2). Small randomly distributed carbide particles, not completely resolved by optical microscopy, are present in the bainitic matrix, probably Mo and V carbides. The previous austenite grain boundaries are clearly evident (Fig. 2c,d), probably due to the occurrence of a precipitated carbides layer, not always

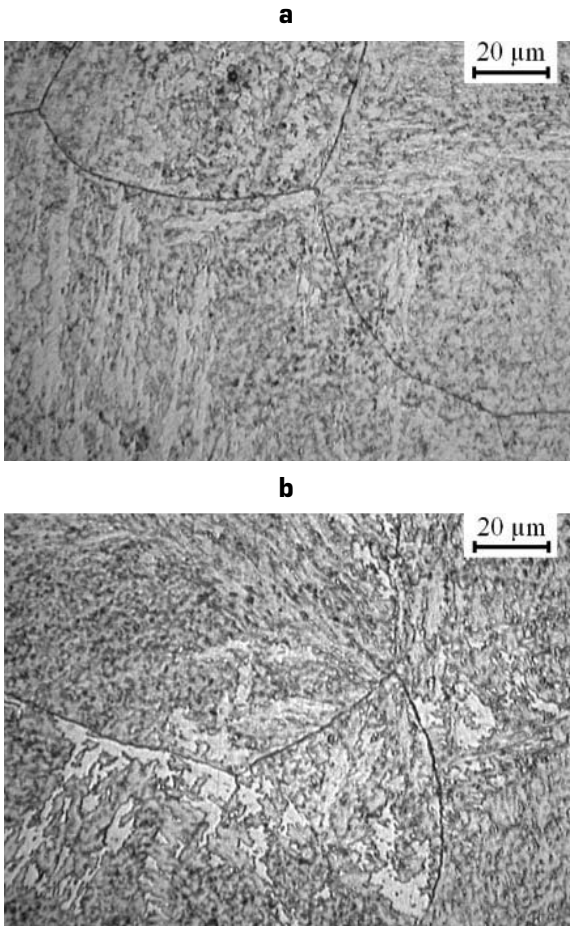

Fig. 3

Microstructures after aging for about 330 min (from as-received condition) at 470 °C (a) and 550 °C (b); temper modified bainite.

Microstrutture dopo invecchiamento per circa 330 min. (dalla condizione di fornitura) a 470 °C (a) e 550 °C (b); bainite modificata dal rinvenimento.

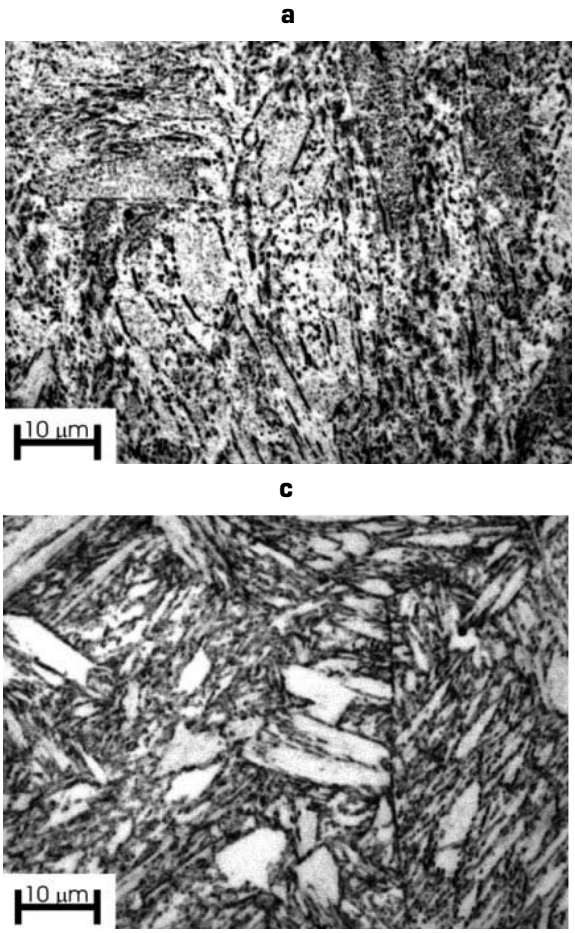

Fig. 4

Re-heat-treated samples microstructure (water quenching and double tempering at 400°C) (a). Microstructure after further aging for 330 min. at 470 °C (b), 510 °C (c) and 550 °C (d). Tempered martensite.

Microstruttura dei campioni ritrattati (tempra in acqua e doppio rinvenimento a 400 °C) (a). Microstrutture dopo i successivi trattamenti di invecchiamento per 330 min. a 470 °C (b), 510 °C (c) e 550 °C (d). Martensite rinvenuta.

continuous, and partially removed during the metallographic preparation. The average austenitic grain size is 130 μm (mean of 263 intercepts).

As it regards the laboratory re-heat-treatment, after water quenching, a martensitic microstructure with lath morphology (typical of low carbon steels) was obtained. The microstructure exhibits 445 HV_{100} hardness and 980 MPa yield strength (determined by FIMEC test). The tempered martensite, obtained after the first tempering at 400 °C, exhibited a morphology similar to the previous as-quenched martensite, but with a lower hardness (420 HV_{100}) and yield strength (910 MPa, by FIMEC test). Both the microstructure and these mechanical properties did not change noticeably after the second tempering.

The optical metallographic analysis of as received samples has not detected important microstructural variation after aging (Fig. 3).

The previous austenite grain boundary precipitates, observed in the as-received samples, are not present in the re-heat treated samples, neither after the quenching nor after the double tempering at 400 °C (Fig. 4a); however, they are again visible, in increasing amount, after aging the re-heat-treated samples at temperatures increasing from 470 to 550 °C (Fig. 4b,c,d).

Detailed SEM examination of aged samples (initially being either in the as-received or in the re-heat-treated condition) showed that the amount of detectable carbides mostly decreases with the aging duration and temperature (Fig. 5); therefore, it is hypothesized that during the aging treatments the previously existing carbides, formed during the previous heat treatments and probably not thermodynamically stable in the aging temperature range, are progressively solubilized, while finer (undetectable) carbides, possibly with a different composition, are re-precipitated and may be the origin of the detected hardness increase (see below).

The X-ray analysis of the second phases (carbides and inclusions) electrochemically extracted from the re-heat-treated sample aged at 550 °C for 440 min is displayed in Fig. 6. The most important diffraction peaks can be attributed to the η-MoC carbide, with the possible presence of the V_7C_8 carbide. Moreover, the EDS analysis, carried out on the same second phases compacted powder, has confirmed the occurrence of molybdenum, that has the highest peak, and of

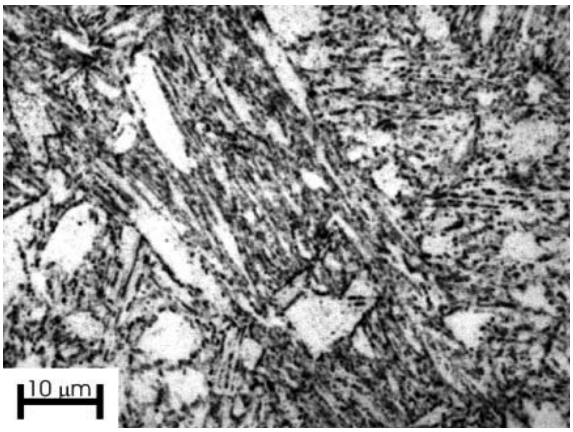

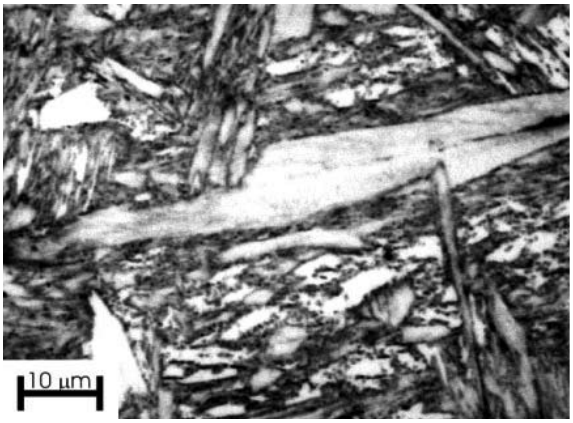

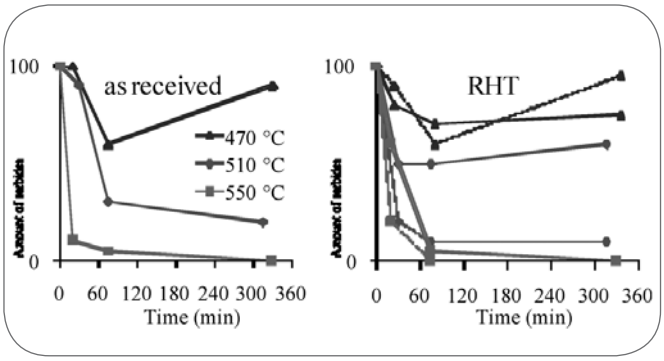

Fig. 5

Amount of detectable carbides (from SEM observations) during aging of either as-received or re-heat-treated samples, as a percentage of the amount observed before aging, as a function of the aging duration and temperature, for different carbide morphologies (continuous lines - elongated carbides, and dashed lines - small carbides).

Quantità di carburi rilevabili (da osservazioni SEM) durante l'invecchiamento di campioni o in stato di fornitura, o ri-trattati, come percentuale della quantità osservata prima dell'invecchiamento, in funzione della durata e temperatura dell'invecchiamento, per diverse morfologie dei carburi (linee continue - carburi allungati e linee tratteggiate - carburi piccoli).

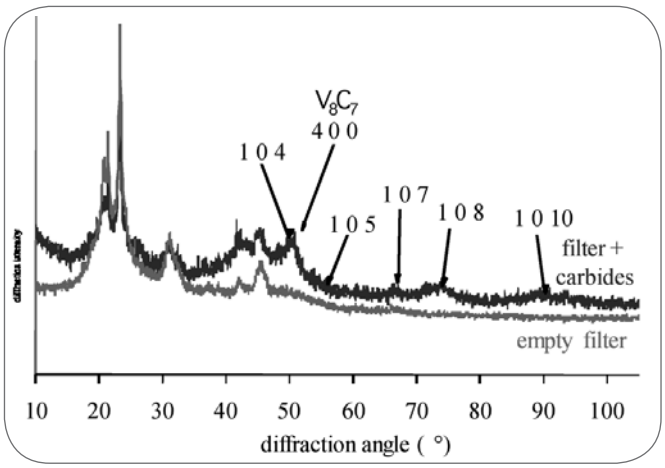

Fig. 6

Filter and filter-plus-carbides diffraction spectra of re-heat treated sample aged at 550 °C for 440 min; diffraction peaks of η-MoC (PDF # 08-0384) and V_8C^7 (PDF # 35-0786).

Spettri di diffrazione di un filtro vuoto e del filtro con carburi del campione ri-trattato ed invecchiato a 550 °C per 440 min; picchi di diffrazione di η-MoC (PDF # 8-384) e V_8C_7 (PDF # 35-786).

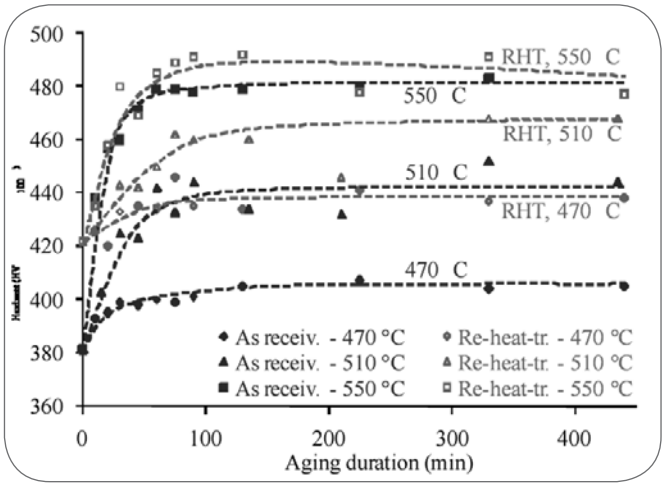

Fig. 7

Effect of the aging temperature and duration on the hardness of the as received and re-heat-treated material.

Effetto della temperatura e della durata dell'invecchiamento sulla durezza del materiale allo stato di fornitura e ri-trattato.

others elements, such as V, Fe, Cr, Si.

Mechanical tests

The results of the tensile and fracture toughness tests are listed in Tab. 2 and 3, and compared with the previously assessed properties of the ISO 1.2738 steel [2]. In particular, the fracture toughness value of the examined steel in the as-received condition is somewhat higher than that of the ISO 1.2738 steel, whereas the tensile properties are comparable.

The hardness curves relative to the age hardening heat treatment on the as-received and re-heat-treated samples are displayed in Fig. 7. The 550 °C aging temperature yielded the

Condition / steel	YS MPa	UTS MPa	n -	El_u %	El_t %
As-received (A.r.)	855	1156	0.13	8.7	15
A.r. + Aged 470 °C	817	1233	0.16	9.2	12.1
A.r. + Aged 510 °C	1054	1331	0.12	6.3	7.6
A.r. + Aged 550 °C	1225	1417	0.14	2.4	1.1
RHT + aged 470 °C	1062	1288	0.10	5.2	13.6
RHT + aged 510 °C	1154	1356	0.09	4.6	12.9
RHT + aged 550 °C	1302	1457	0.10	2.8	12.0
1.2738 surface	953	1092	0.10	7.0	14
1.2738 core	665	983	0.17	8.8	15.7

Tab. 2

Tensile properties of the examined steel, in different metallurgical conditions, compared with the 1.2738 steel (average values for each steel or position). YS: Yield Strength; UTS: Ultimate Tensile Strength; n: hardening exponent; El_u uniform elongation; El_t elongation at fracture. Aging duration 2.5 h.

Proprietà tensili dell'acciaio esaminato, in diverse condizioni metallurgiche, confrontato con l'acciaio 1.2738 (valori medi per ciascun acciaio o posizione). YS: tensione di snervamento; UTS: tensione di rottura; n: esponente di incrudimento; El_u allungamento uniforme; El_t allungamento a rottura. Tempo di invecchiamento 2,5 h.

Condition / steel	Fracture toughness MPa√m
As-received (A.r.)	70
A.r. + Aged (3 h at 525 °C)	43
1.2738 surface	35
1.2738 core	45

Tab. 3

Fracture toughness (KIc) of the examined steel, in different metallurgical conditions, compared with the 1.2738 steel (average values).

Tenacità a frattura (KIc) dell'acciaio esaminato, in diverse condizioni metallurgiche, confrontato con l'acciaio 1.2738 (valori medi).

highest hardness values: 490 HV_{100} for the re-heat treated sample and 485 HV_{100} for the as-received one, starting from 420 and 380 HV_{100}, respectively. As a consequence, the as-received specimens are more sensitive to the aging heat treatment than the re-heat-treated ones, achieving a similar hardness notwithstanding their hardness being less before aging. Probably, this behavior is due to the fact that the hardness of the bainitic and martensitic microstructure (of the as-received and re-heat treated samples, respectively) progressively becomes similar at increasing aging temperature, due to supplementary tempering phenomena superimposing on the aging precipitation. Overaging phenomena are not detected, except that in the re-heat treated sample aged at 550 °C, which exhibits a slight decrease in hardness for duration longer than 3 hours.

The FIMEC stress vs. displacement curves, obtained on the as-received and re-heat treated samples aged for the longest durations (about 440 min, Fig. 8), confirm the above results: the yield stress (like the hardness) increases from 890 MPa in the as-received condition, to 1230, 1275 and 1375 MPa, after aging at 470, 510 and 550 °C, respectively; the as-received and re-heat treated FIMEC curves become similar at increasing aging temperature, and those pertaining to the highest aging temperature are consistent with the slight overaging observed in the re-heat treated samples (Fig. 7).

Charpy impact notch tests were carried out as a function of temperature on the as-received and re-heat-treated samples, the latter being either not aged, or aged at 520 °C for 2 h. (Fig. 9). The laboratory re-heat-treatment noticeably decreases the brittle to ductile transition temperature, which anyway remains above the room temperature (Fig. 9). The fracture surfaces appearance, in the center of the samples, is always brittle and consists mainly of cleavage zones.

The results of the tensile tests performed on the as-received and re-heat treated specimens after aging at 470, 510 and 550 °C for 2.5 h are displayed in Tab. 2 and in Fig. 10. As expected, aging at increasing temperatures yields higher yield and tensile strength, but lower uniform and fracture elongation. Consistently with the aforementioned hardness measurements (Fig. 7), aged as-received and aged re-heat-treated specimens have different uniform elongation, yield and tensile strength, for the same aging temperature, but these differences decrease at increasing aging temperature. On the contrary, the elongation-to-fracture difference increases; in particular, the aged as-received samples fail in a brittle manner, without appreciable necking. The lower toughness of the as-received and aged condition is confirmed by a significant reduction of the fracture toughness after aging, from 70 to 43 MPa√m (Tab. 3). The plane-strain fracture surface of the as-received material

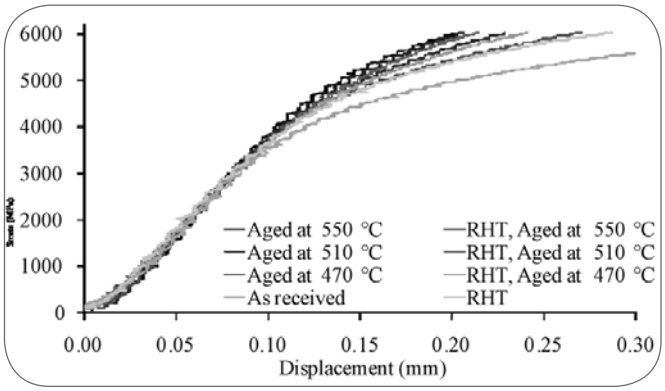

Fig. 8

FIMEC flat indentation stress-displacement curves. As-received and re-heat-treated (RHT) specimens before and after aging for about 440 min at 470, 510, or 550 °C.

Curve tensione spostamento dell'indentazione piana FIMEC. Campioni in stato di fornitura e ritrattati (RHT) prima e dopo l'invecchiamento per circa 440 min a 470, 510 o 550 °C.

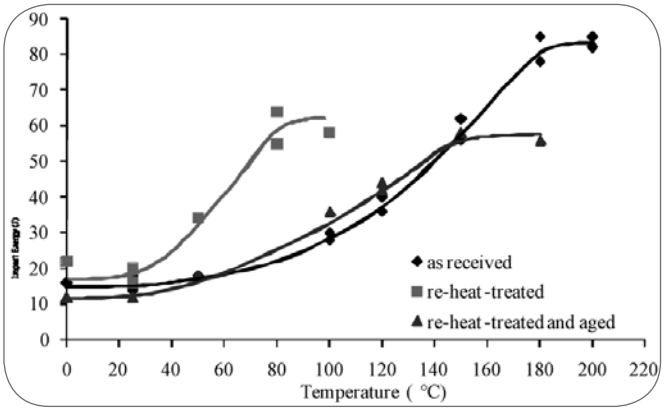

Fig. 9

Charpy-V impact tests: brittle-to-ductile transition curves of the as-received, re-heat-treated, and re-heat-treated and aged (at about 520°C for 2 h) metallurgical conditions.

Prove di resilienza Charpy-V: curve di transizione fragile-duttile dei campioni in condizioni metallurgiche di fornitura, ri-trattata, e ri-trattata ed invecchiata (a circa 520 °C per 2h).

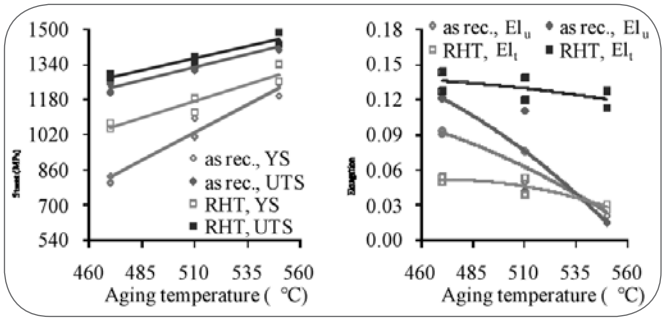

Fig. 10

Tensile properties of aged samples (from initial as-received and re-heat treated, RHT, condition). Yield Strength (YS) and Ultimate Tensile Strength (UTS), elongation to fracture (El_t) and uniform elongation (El_u).

Proprietà tensili di campioni invecchiati (dalle condizioni iniziali di fornitura, as. rec., o di ri-trattamento, RHT). Tensione di snervamento (YS) e di rottura (UTS), allungamento a rottura (El_t) ed allungamento uniforme (El_u).

shows mainly cleavage facets (Fig. 11a,b), with small ductile intergranular rupture areas (Fig. 11b); the latter morphology becomes prevalent in the as-received tensile fracture surface, together with some cleavage (Fig. 12).

Overall, the morphology of the tensile fracture surfaces of the different examined aged conditions depend mainly on the metallurgical state before the aging heat treatment. In fact, both the aged and not-aged as-received samples exhibit cleavage areas and ductile intergranular rupture areas (consistently with the lack of necking, Fig. 12a,c,e), whereas the fracture surfaces of the re-heat-treated and aged samples always show a cup-and-cone morphology, with mode-I coalesced micro-voids and mode-II shear areas (Fig. 12b,d).

DISCUSSION AND CONCLUSIONS

The microstructure of the examined positions inside the steel bloom consists almost completely of bainite modified by tempering. Therefore, the bloom fracture toughness is low in comparison to usual quenched and tempered steels, being about

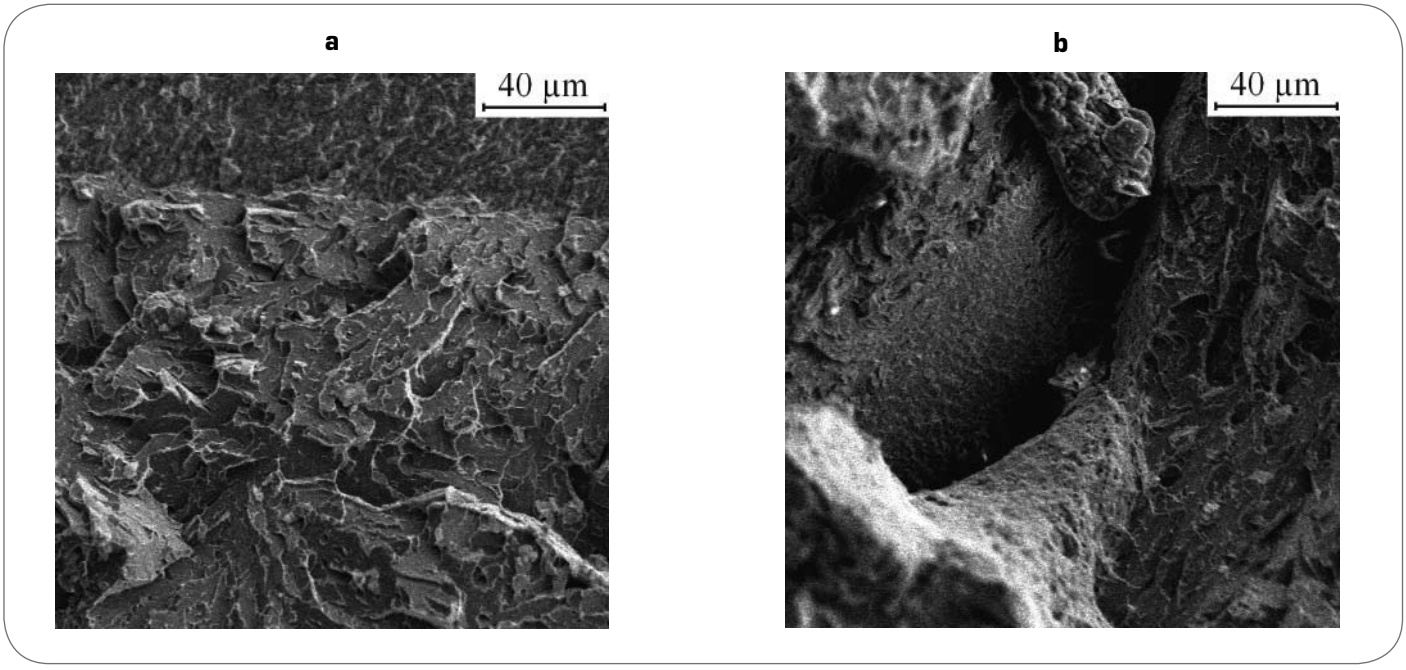

Fig. 11

Plane-strain fracture surfaces in the as-received steel, at the onset of metastable crack propagation (a) and in the crack propagation region (b).

Superfici di frattura in deformazione piana nell'acciaio in stato di fornitura, all'inizio della propagazione instabile (a) e nella regione di propagazione instabile (b).

a

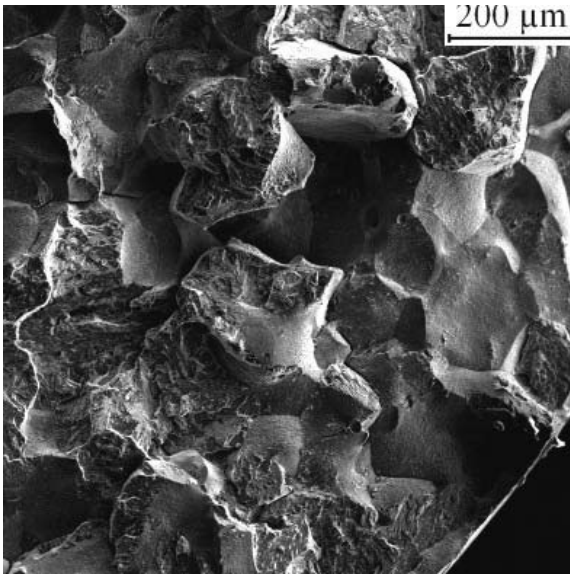

b

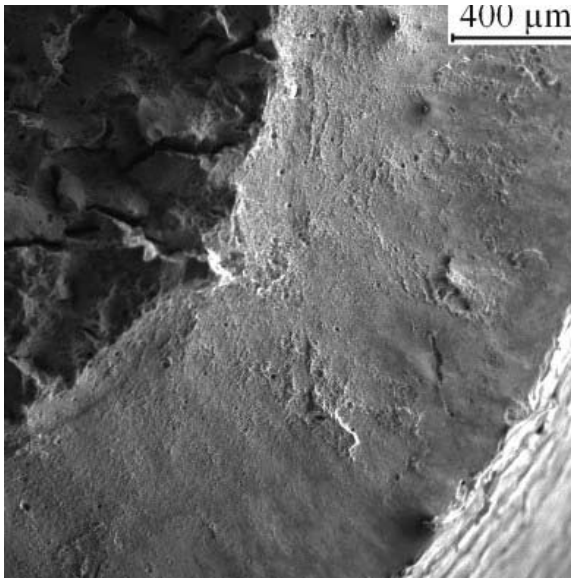

c

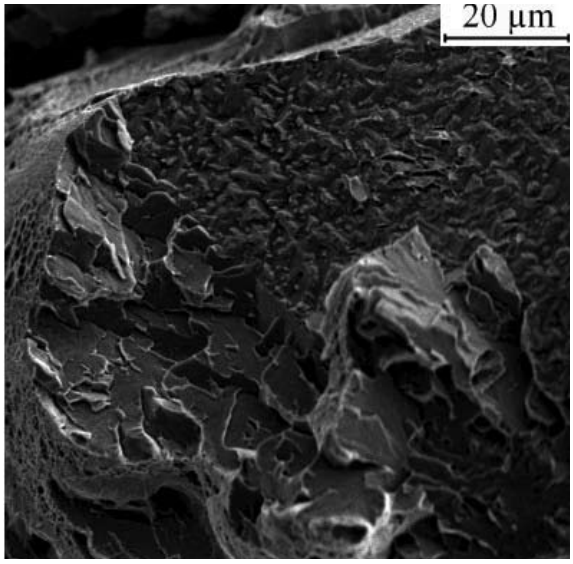

d

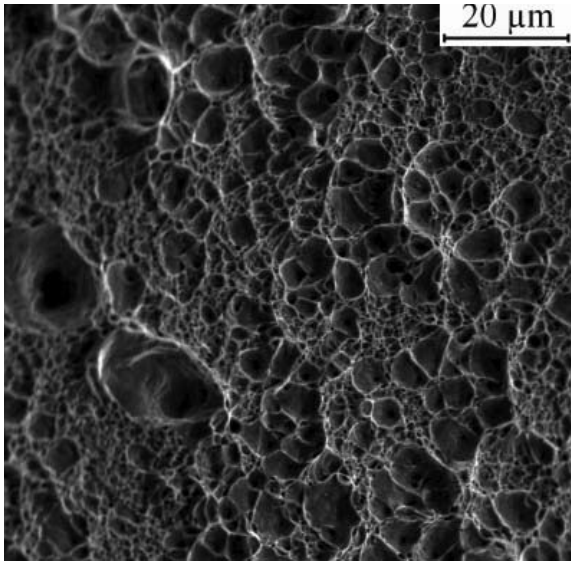

d

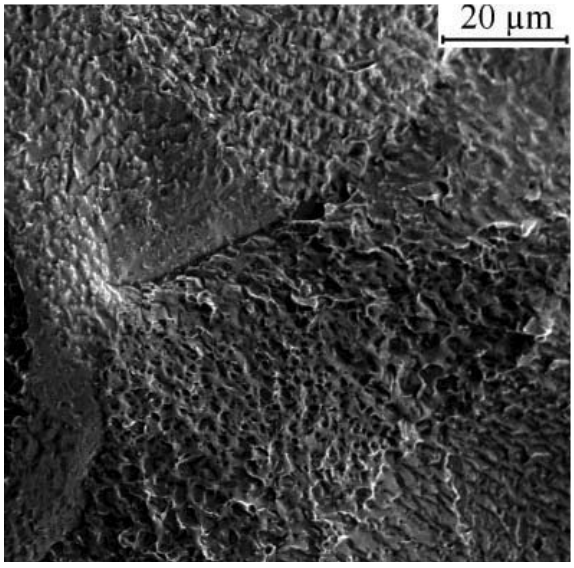

◀ Fig. 12

Tensile fracture surface of as-received (a,c,e) and re-heat-treated (b,d) steel, after aging at 550 °C. Overviews (a,b) and details (c,d,e).
Superfici di frattura a trazione dell'acciaio in stato di fornitura (a,c,e) e ri-trattato (b,d), dopo invecchiamento a 550 °C. Viste complessive (a,b) e dettagli (c,d,e).

70 MPa√m, but somewhat higher in respect to the largely used 1.2738 steel (40 MPa√m on average).
The as-received steel shows a precipitates layer at the previous austenitic grain boundaries, which may be tentatively related with the ductile intergranular fracture observed after the tensile tests in the as-received, both not-aged and aged, samples. Nevertheless, the aged re-heat-treated tensile specimens present fully ductile fracture surfaces, even if they also show a similar precipitates layer at the austenitic grain boundaries after the aging treatment (although not after the re-heat-treatment). Therefore, the possible relationship among the grain-boundary precipitates and the intergranular rupture is not yet completely clear.
The as-received specimens are more sensitive to the aging heat treatment than the re-heat-treated ones, since they yield increasingly similar hardness values after aging at increasing temperatures, notwithstanding their lower hardness before aging. This fact may be partially explained by hypothesizing that the initial differences between the bainitic and martensitic matrixes (already tempered at low temperature) are progressively reduced due to coalescence phenomena occurring during tempering at increasing temperatures and interferring with the precipitation during aging.
The FIMEC and tensile tests of aged and not aged samples overall confirm the results of the hardness versus aging duration tests; moreover, the tensile tests evidence a difference in the fracture mode between the as-received and aged samples and those re-heat-treated and aged, the former generally showing brittle fracture surfaces without significant necking, and the latter ductile fracture surfaces and evident necking. Therefore, and also by considering the reduction of fracture toughness (43 MPa√m) of the as-received steel after aging at 525 °C, it is concluded that the aging treatment generally causes a relevant toughness reduction.
Overall, the reported results, and particularly the hardness curves as a function of the aging duration, outline the kinetics of the aging process and constitute a data set that could be employed for the choice of the more suitable parameters (duration and temperature) for the aging treatment of specific molds. In particular, the substantially asymptotic trend of the hardness, as a function of the aging duration, at the examined temperatures and for durations up to 8 h, may allow to obtain homogeneous result also in the aging of molds with large cross-section, for which the actual duration at temperature is necessarily differentiated from surface to core.
Nevertheless, the nature of the metallurgical transformations that originate the hardening process has not been completely determined yet and will be the subject of further studies. A first hint in this direction is given by the observation of the gradual disappearance of the previously existing carbides during the aging treatments, which may be related with the precipitation of different, finer carbides.

ACKNOWLEDGEMENTS

Italian Ministry for University and Research, for financial support by research grant PRIN 2005090102. Lucchini Sidermeccanica steelwork, Lovere, Italy, for steel procurement and the CCT diagram.

REFERENCES

1] ISO 4957:1999, Tool steels. ISO, 1999.
2] D. Firrao, P. Matteis, G. Scavino, G. Ubertalli, M.G. Ienco, M.R. Pinasco, E.Stagno, R.Gerosa, B. Rivolta, A. Silvestri, G. Silva, A. Ghidini. Relationships between tensile and fracture mechanics properties and fatigue properties of large plastic mould steel blocks. Materials Science and Engineering A, 468-470 (2007), 193-200.
3] N. Bailey, F.R. Coe. Welding steels without hydrogen cracking (Cambridge, Abington publ: 1973).
4] A.M. Bayer, T. Basco, L.R. Walton. Wrought tool steels, in: Metals handbook - 10th Ed. - Vol. 1 - Properties and selection: irons, steels and high performance alloys, curatori J.R. Davis et al. (Materials Park, OH, USA: A.S.M. Int., 1990) 757-779.
5] G.A. Roberts, R.A. Cary. Tool steels. (Metals Park, OH, USA: ASM, 1980).
6] T. Schade, Steel Selection - Closing the Gap with Offshore Tooling, MoldMaking Technology Magazine, Ott. 2003.
7] P.M. Unterweiser, H.E. Boyer, J.J. Kubbs (curatori). Heat Treaters's Guide: Standard Practices and Procedures for Steel (Metals Park, OH, USA: American Society for Metals, 1982).
8] C.C. Davis. Selection of Materials for Molds for Plastics and Rubbers, in: Metals Handbook, 9th Ed., Vol. 3, Properties and selection: stainless steels, tool materials and special purpose metals, curatori W.H. Cubberly et al. (Metals Park, OH, USA: A.S.M., 1980) 546-550.
9] M. Faccoli, A. Ghidini, R. Roberti. A Study of the strengthening mechanisms in the novel precipitation hardening keylos 2001 steel, in: Proceedings of 7th international tooling conference - Tooling materials and their applications from research to market - Politecnico di Torino – Torino, Italy, 2-5 may 2006, curatori M. Rosso, M. Actis Grande, D. Ugues (Milano: Ancora, 2006), Vol. 2, 153-161.
10] E407-99, Standard Practice for Microetching Metals and Alloys", ASTM, 1999.
11] E112-96. Standard test methods for determining average grain size. ASTM, 1996.
12] S. Bechet, L. Beaujard. Nouveau réactif pour la mise en évidence micrographique du grain austénitique des aciers trempés ou trempés - revenus," La Revue de Métallurgie, 52 (1955), 830.
13] E399-05. Standard test method for plane-strain fracture toughness of metallic materials. ASTM, 2005.
14] A. Donato, P. Gondi, R. Montanari, L. Moreschi, A. Sili, S. Storai. A remotely operated FIMEC apparatus for the mechanical characterization of neutron irradiated materials. Journal of Materials Science, 258-263 (1998), 446-451.
15] R. Mouginot, D. Maugis. Fracture indentation beneath flat and spherical punches, Journal of Materials Science, 20 (1985), 4354-4376.
16] H.Y. Yu, M.A. Imam, B.B. Rath. Study of the deformation behaviour of homogeneous materials by impression tests, Journal of Materials Science, 20 (1985), 636-642.
17] P. Gondi, R. Montanari, A. Sili. Small-scale nondestructive stress-strain and creep tests feasible during irradiation, Journal of Nuclear Materials, 212-215 (1994), 1688-1692.

ABSTRACT

EFFETTO DEL TRATTAMENTO TERMICO SULLE PROPRIETÀ MECCANICHE DI UN ACCIAIO INDURENTE PER PRECIPITAZIONE PER GRANDI STAMPI PER MATERIE PLASTICHE

Parole chiave: acciaio, precipitazione

Gli stampi per particolari in materia plastica di grande dimensione, quali per esempio paraurti e cruscotti, usati nell'industria automobilistica, sono solitamente lavorati per asportazione di truciolo da grandi blocchi di acciaio prebonificato. I blumi di acciaio ISO 1.2738 tradizionalmente usati presentano microstrutture disomogenee e tenacità ridotta ($K_{Ic} \approx 40$ MPa√m e KV ≈ 10 J a temperatura ambiente); inoltre questo acciaio è difficilmente saldabile ($C_{eq} \approx 1{,}16$). Numerosi acciai indurenti per precipitazione sono stati proposti come alternativa per superare questi limiti.

Siccome i processi di indurimento per precipitazione inducono deformazioni molto limitate, possono essere svolti dopo la lavorazione meccanica. Inoltre, questi processi possono produrre microstrutture e proprietà meccaniche omogenee in stampi grandi e geometricamente complessi.

È stato esaminato un acciaio induribile per precipitazione sviluppato per la fabbricazione di stampi per materie plastiche, con la composizione chimica esposta in Tabella I. Il ciclo produttivo consiste di colata, forgiatura, trattamento termico iniziale (svolto in acciaieria), lavorazione meccanica ed indurimento per invecchiamento. Il trattamento termico iniziale consiste di un trattamento preliminare (includente una de-idrogenazione) seguito da austenitizzazione/solubilizzazione a 1020 °C, tempra in aria e doppio rinvenimento a 400 °C (Fig. 1); questo trattamento è rivolto ad ottenere una microstruttura bainitica con durezza compresa tra 310 e 350 HB.

Un blumo di dimensione originale 500x1500x2400 mm è stato esaminato allo stato di fornitura, cioè dopo il trattamento termico iniziale sopra descritto. Inoltre, alcuni campioni sono stati ritrattati in laboratorio come segue: austenitizzazione/solubilizzazione a 1050 °C, tempra in acqua, doppio rinvenimento a 400 °C, ottenendo martensite rinvenuta.

Il rafforzamento per precipitazione è stato studiato usando campioni inizialmente o allo stato di fornitura, o ritrattati in laboratorio, e poi invecchiati a 470, 510 o 550 °C per durate fino ad 8 h.

Le microstrutture sono illustrate nelle Fig. 2, 3 e 4. La dimensione del grano austenitico allo stato di fornitura è di 130 µm. Carburi precipitati presso i bordi di grano austenitici sono presenti allo stato di fornitura, assenti allo stato ri-trattato, e nuovamente presenti allo stato ritrattato ed invecchiato. La quantità di carburi osservati mediante SEM decresce all'aumentare della temperatura e durata dell'invecchiamento (Fig. 5); si ipotizza che i carburi esistenti agli inizi degli invecchiamenti siano gradualmente solubilizzati, permettendo la precipitazione di altri carburi più fini, non osservabili, che causano il rafforzamento. L'analisi XRD dalle seconde fasi, estratte per via elettrochimica (da un campione ri-trattato ed invecchiato a 550 °C, Fig. 6), evidenzia la presenza di η-MoC e la possibile presenza di V_7C_8.

Allo stato di fornitura la durezza e le proprietà tensili sono paragonabili a quelle dell'acciaio ISO 1.2738, ma la tenacità a frattura è maggiore (Tab. II e III); la frattura in deformazione piana avviene per clivaggio (Fig. 11). Il ritrattamento termico riduce sensibilmente la temperatura di transizione fragile-duttile (Fig. 9). Gli invecchiamenti incrementano notevolmente la durezza (Fig. 7); l'incremento è maggiore per i campioni allo stato di fornitura, la cui durezza iniziale è minore; per le temperature e durate esaminate il sovrainvecchiamento è assente o trascurabile. Questi risultati sono confermati anche da prove di indentazione strumentata con penetratore cilindrico (FIMEC, Fig. 8). L'invecchiamento a temperature crescenti aumenta le tensioni di snervamento e rottura, coerentemente con l'aumento della durezza (Fig. 10); però i campioni di trazione allo stato di fornitura ed invecchiati si rompono in modo fragile, senza apprezzabile strizione (contrariamente a quelli ritrattati ed invecchiati, Fig. 10 e 12). L'effetto avverso dell'invecchiamento sulla tenacità, nel caso di materiale inizialmente allo stato di fornitura, è confermato dalla riduzione della tenacità a frattura ($K_{Ic} \approx 43$ MPa√m dopo invecchiamento a 525 °C).

Nel loro insieme, i risultati esposti illustrano la cinetica e gli effetti del processo di invecchiamento e costituiscono un insieme di dati utili per scegliere i parametri di invecchiamento più adeguati per specifici stampi.